Quantum-enhanced metrology based on Fabry-Perot interferometer by squeezed vacuum and non-Gaussian detection

Wenfang Li, Jinjin Du, Ruijuan Wen, Gang Li, and Tiancai Zhang[a)]
State Key Laboratory of Quantum Optics and Quantum Optics Devices, Institute of Opto-Electronics, Shanxi University, Taiyuan 030006, China

(Received 19 February 2014; accepted 12 March 2014; published online 27 March 2014)

We have investigated the transmission spectra of a Fabry-Perot interferometer (FPI) with squeezed vacuum state injection and non-Gaussian detection, including photon number resolving detection and parity detection. In order to show the suitability of the system, parallel studies were made of the performance of two other light sources: coherent state of light and Fock state of light either with classical mean intensity detection or with non-Gaussian detection. This shows that by using the squeezed vacuum state and non-Gaussian detection simultaneously, the resolution of the FPI can go far beyond the cavity standard bandwidth limit based on the current techniques. The sensitivity of the scheme has also been explored and it shows that the minimum detectable sensitivity is better than that of the other schemes. © *2014 AIP Publishing LLC*.
[http://dx.doi.org/10.1063/1.4869455]

It is well known that the fundamental limits of measurement precision are basically determined by the Heisenberg uncertainty principle. These limits are impossible to be exceeded by conventional measurement strategies. Conventional limits such as the shot noise limit (SNL) or the standard quantum limit (SQL) to the precision measurements can be surpassed by using quantum technique, such as squeezed states and entangled states.[1–3] Since the beginning of generation of squeezed states, considerable effort has gone into expanding it to various precision measurements, which lies at the heart of modern science and engineering.[4] Quantum metrology is to study all kinds of quantum techniques that enable one to gain advantages over purely conventional approaches.[5] With the variety of quantum light sources to hand, quantum optics has been making impressive advances in exploring ultra-high precision measurement beyond the SQL[6] or even Heisenberg limit (HL).[1,7,8] In the past decade, quantum metrology,[9] as the emerging interdisciplinary field, has shown the potential to impact not only on fundamental science but also precision measurement technology.

There are several approaches to improve the precision of the measurement in SU(2) interferometer. The first one is to use the quantum-light sources directly. For example, a well-known strategy is to use the squeezed vacuum to inject the unused port of the interferometer[10,11] to improve the measurement precision, which has been applied to gravitational wave detection in the project of Laser Interferometer Gravitational Wave Observatory (LIGO).[12,13] With the development of optical techniques, large squeezing of vacuum state with 12.3 dB has been generated experimentally[14] and in the foreseeable future, even higher squeezing could be achieved and the actual application of such quantum light sources may be feasible. Here, the focus is turned away from unavailable state such as NOON state with large mean photon number and related state with current technology and instead of the use of the squeezed vacuum state (SVS).

The second approach is to use quantum detection, such as photon number resolving detection (PNRD), the typical non-Gaussian measurement, in contrast to the classical mean intensity detection (MID). Recent optical detection by the transition edge sensor (TES) technique has provided the photon number resolving method with high detection efficiency.[15] This TES has been introduced in the Fabry-Perot interferometer (FPI) to exceed classical detection.[16] As the development of photon detection technique progresses, TES may be widely used in the field of quantum optics and quantum metrology.[17]

In this paper, the resolution and sensitivity of the usual FPI are explored by using both approaches simultaneously, i.e., the quantum light source and the quantum detection method. The result shows that the resolution of the FPI is beyond the SQL given by coherent state (CS) injection with conventional classical detection, even better than that by Fock state (FS) with PNRD. It is striking that the numerical calculation shows that the sensitivity of the FPI, corresponding to the sensitivity of length or frequency the FPI can sense, is even better than that of the Heisenberg limit for small photon numbers. The calculation is based on the state-of-the-art technology of the SVS with PNRD and parity detection (PD), and the scheme is feasible for physical implementations.

Consider the standard FPI in Fig. 1(a). Specifically, a symmetric cavity with length L is introduced, i.e., both input and output mirrors have the identical reflection and transmission coefficients r' and t'. Quantum mechanically, the whole FPI can be regarded as a black box with the input modes $\hat{a}_1$ being a quantum or classical light beam on the one port and a vacuum input of $\hat{a}_2$ from the other, and the corresponding two output modes $\hat{a}_3$ and $\hat{a}_4$, respectively. Thus, the system is equivalent to an effective beam-splitter (BS) transformation shown in Fig. 1(b).

[a)]Electronic mail: tczhang@sxu.edu.cn

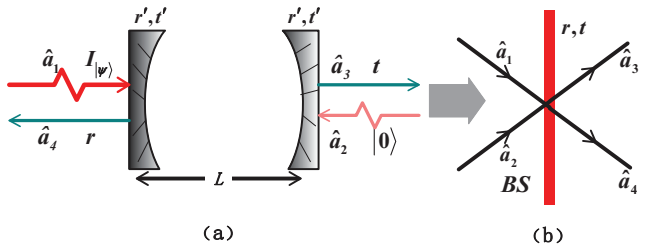

FIG. 1. (a) Fabry-Perot interferometer with complex amplitude r' and t' for reflection and transmission coefficients of the input and output mirrors, respectively. (b) The system is equivalent to an effective BS transformation. The effective BS has the complex amplitudes t and r for the input and output modes.

In general, the relationship between the incoming and the outgoing quantized modes in the effective BS is indicated as

$$\begin{pmatrix} \hat{a}_3 \\ \hat{a}_4 \end{pmatrix} = \begin{pmatrix} t & r \\ r & t \end{pmatrix} \begin{pmatrix} \hat{a}_1 \\ \hat{a}_2 \end{pmatrix}. \tag{1}$$

The transmission and reflection functions t and r are given by[16]

$$t(r',\phi) = \frac{(1-|r'|^2)e^{-2i\sqrt{1-|r'|^2}}}{|r'|^2 e^{-2i\sqrt{1-|r'|^2}} e^{2i\phi} - 1}, \quad \phi = kL = 2\pi L/\lambda, \tag{2}$$

$$r(r',\phi) = \frac{|r'|e^{-i\sqrt{1-|r'|^2}}\left(e^{-i\phi} - e^{i\phi}e^{-2i\sqrt{1-|r'|^2}}\right)}{|r'|^2 e^{-2i\sqrt{1-|r'|^2}} e^{2i\phi} - 1}, \tag{3}$$

where r' signifies the complex reflectivity of the mirrors and the phase ϕ is determined by the wavenumber K of the incoming light and the cavity length L.

For this FPI, there are four configurations according to the injection states and the detection methods, shown in Table I. For the input states, we can choose either the classical states, such as CS or quantum states, such as FS and SVS.[18] For the detection methods, either the classical detection (CD), such as the MID which detects the average photon $\langle a^+ a\rangle$ can be used, or the quantum detection, such as the non-Gaussian detection of PNRD, which detects the exact photon k, corresponding to the projection operator $\hat{C} = |k\rangle\langle k|$, or the PD, which judges the even or odd number of the impinging light, corresponding to the detection operator $\hat{\Pi} = (-1)^{\hat{n}}$.[1,19–21] So far, both the PNRD and PD by TES[22] or single photon counting module (SPCM) or multiple SPCMs[23,24] have been utilized in experiments, and the parity detection is feasible, either by optical nonlinearities[19] or the measurement of Wigner function at the origin.[21]

TABLE I. Different combinations for measuring the transmission spectra of FPI.

Detection strategies	Input states	Detection method	Detected photon expectation
CC	CS	MID	$P_C^{CS} = \bar{n}\lvert t\rvert^2$
QC	SVS		
		MID	$P_C^{SVS} = \bar{n}\lvert t\rvert^2; P_C^{FS} = n\lvert t\rvert^2$
	FS		
CQ		PNRD	$P_k^{CS} = \frac{e^{-\lvert\alpha\rvert^2\lvert r\rvert^2}\lvert r\rvert^{2k}\lvert\alpha\rvert^{2k}}{k!}$
	CS		
		PD	$P_{PD}^{CS} = e^{-2\lvert r\rvert^2\lvert\alpha\rvert^2}$
QQ	SVS		See Eq. (5)
		PNRD	See Eq. (6)
		PD	$P_k^{FS} = \frac{n!}{(n-k)!k!}\lvert t\rvert^{2k}\lvert r\rvert^{2(n-k)}$
	FS		$P_{PD}^{FS} = (1-2\lvert t\rvert^2)^n$

Table I shows the transmission spectra of the four types of detection strategies. Here, it has been assumed that the reflectivity of the input and output mirrors is 70%. The first column states the detection strategies: C means classical state (or classical detection method) and Q means quantum state (or quantum detection method). So there are four combination: classical state with classical detection (CC), quantum state with classical detection (QC), classical state with quantum detection (CQ) and quantum state with quantum detection (QQ). The second column lists a few specific examples corresponding to the first column with CS, FS, and SVS as input resources. MID, PD, and PNRD in the third column provides the detection methods. Once the input state and the detection method are given, one can obtain the detection photon expectation given in the fourth column, where $P_D^{|\psi\rangle}$ is the detected photon expectation by means of detection method D with the state of $|\psi\rangle$.

The corresponding normalized transmission spectra can be obtained by calculating the average intensity output of the interferometers. The normalization probability is

$$P = \frac{1}{\bar{n}}\sum_{k=1}^{\infty} k \cdot P_k^{CS} = \frac{1}{\bar{n}}\sum_{k=1}^{\infty} k \cdot P_k^{SVS} = |t|^2. \tag{4}$$

This normalized probability corresponding to the input of CS and the detection of MID, which sets the standard resolution and sensitivity of this FPI, cannot be improved upon by any classical light sources with any traditional classical detection methods. Thus, a cavity natural bandwidth (CNB) can be defined, which determines the best resolution of the FPI and the standard quantum sensitivity corresponding to the FPI, as was done by SQL for light noise. This CNB is actually the natural bandwidth of the FPI given by the normalized spectra (4).

We found from the last column of Table I that for classical detection, the spectra are the same for CS, FS, and SVS, which actually give the standard bandwidth and the best resolution of FPI in classical limit. However, for quantum detection, depending on the input states, the standard bandwidth can be surpassed. The quantum enhanced FPI quantitatively under the quantum resources and detections will be analysed later.

Now regard the related schemes with SVS of light of mode $\hat{a}_1$ and vacuum state $|0\rangle$ as mode $\hat{a}_2$. The average photon number $\bar{n}$ is determined by the squeezing parameter s for the SVS: $\bar{n} = \sinh^2 s$. The output states of the FPI can be obtained from the initial input states with two modes $|\psi,0\rangle_{\hat{a}_1\hat{a}_2} = |\psi\rangle_{\hat{a}_1}|0\rangle_{\hat{a}_2}$ transferred by the effective BS. By the perfect k-photon detection, the photon number expectation of detecting k photons is given by

$$P_k^{SVS} = Tr(\hat{C}\hat{\rho}^{SVS}) = \frac{1}{\cosh s}\sum_{m=0}^{\infty}[(2m)!]^2|t|^{2k}|r|^{2(2m-k)} \times \frac{(\tanh s)^{2m}}{2^{2m}(m!)^2(2m-k)!k!}. \tag{5}$$

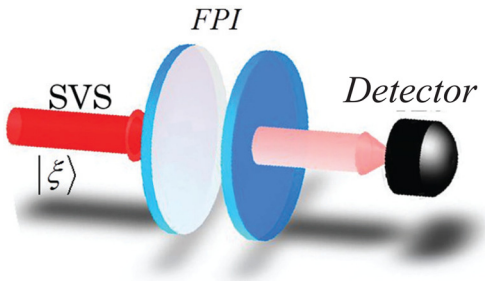

FIG. 2. The scheme of quantum enhanced FPI.

For the PD with parity operator, the photon expectation for PD is similarly given by

$$P_{PD}^{SVS} = \frac{1}{\cosh s}\sum_{m=0}^{\infty}\sum_{k=0}^{2m}[(2m)!]^2|t|^{2(2m-k)}|r|^{2k} \times \frac{(\tanh s)^{2m}e^{i\pi(2m-k)}}{2^{2m}(m!)^2k!(2m-k)!}, \quad (6)$$

where $\hat{\rho}^{SVS}$ denotes the reduced density matrix for the squeezed vacuum state of light in mode $\hat{a}_1$ and the reduced density matrix $\hat{\rho}^{SVS}$ can be obtained from the density operator $\hat{\rho}_{out}$. The schematic diagram is illustrated in Fig. 2.

To clearly show the quantum enhanced features of FPI, the normalized transmission or reflection spectra for various schemes can be analyzed. As an example, the normalized detected spectra $P_D^{|\psi\rangle}$ for all detections with various input states $|\psi\rangle$ are given. The case for $k=3$, $\bar{n}=3$ is shown in Fig. 3. The black line is for "CS + MID" scheme, which gives the CNB of the FPI σ_c, i.e., the full width at half maximum (FWHM). It is observable that the widths of the spectra for both "SVS + PNRD" and "SVS + PD" schemes are much narrower than that of the CNB. The strategy of "SVS + MID" scheme fails to surpass the CNB. Consequently, when both the quantum resource and non-Gaussian measurement are employed simultaneously, the resolution of CNB can be improved upon.

To further demonstrate the improvement of the resolution of the spectra quantitatively, the ratio R is defined as the FWHM $\sigma_D^{|\psi\rangle}$ of the quantum enhanced FPI with the quantum injection state $|\psi\rangle$ and detection approach D over the CNB of σ_c, i.e., $R = \sigma_D^{|\psi\rangle}/\sigma_c$. If R is less than 1, the scheme can exceed the CNB and realize the super-resolution measurement.

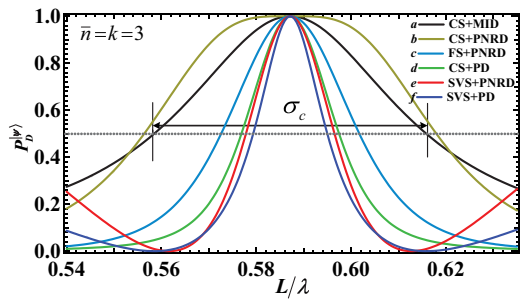

FIG. 3. The normalized $P_D^{|\psi\rangle}$ as a function of L/λ for $\bar{n}=3$ and a photon-number resolved detection for $k=3$. *a* (Black) line: CS + CD (conventional intensity detection); *b* (yellow line): CS + PNRD; *c* (cyan line): FS + PNRD; *d* (green line): CS + PD; *e* (red line): SVS + PNRD; *f* (blue line): SVS + PNRD. The CNB is set as σ_c.

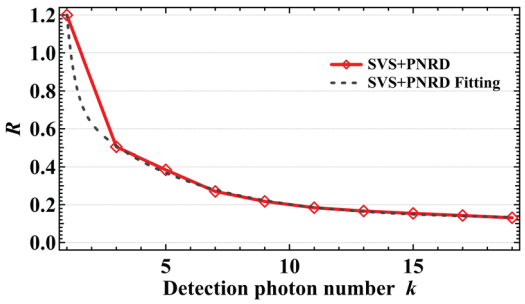

FIG. 4. The ratio of R as the function of the detected photon number for "SVS + PNRD" schemes when the input average photon number is 19. The red diamond line denotes the "SVS + PNRD" scheme and the dashed black line is for fitting (see Ref. 25). The expected lowest value of R is 0.12 when k approaches infinity.

To investigate the capability of improving upon the CNB with "SVS + PNRD" scheme, the ratio R is shown as a function of detected photon number $k(k=1,3,\ldots 19)$ with the fixed average number $\bar{n}=19$ in Fig. 4. The parameter R becomes lower with the increasing k. The spectra are too complicated to give an analytical expression of the limit.[25] Briefly speaking, the scheme enables to achieve super resolution detection for the detection photon number $k>1$.

The dependence of R on the input photon number is also investigated by Fig. 5. Considering the scheme of SVS with two quantum detections (PNRD and PD) and FS with the PNRD, both of them can realize the super resolution and R degrades with the increasing input photon number. Here, the scheme utilizing the SVS shows some advantage over that of the FS by means of PNRD and the anticipated best results of R can be reduced to $R=0.094$.[26]

From all the above results, it can be concluded that the resolution of FPI can be enhanced either by "SVS + PNRD" or "FS + PNRD" and both are better than the CNB. However, on the whole, the best performance of quantum-enhanced resolution for FPI is obtained for "SVS + PD" scheme, which can reduce the ratio R by one order of magnitude. This quantum-enhancement effect is different for the detection method of PNRD and PD for the same input quantum state. It should also be mentioned that without the non-Gaussian detection, one cannot realize the super-resolution measurement even if the nonclassical state such as SVS is introduced for this FPI system.

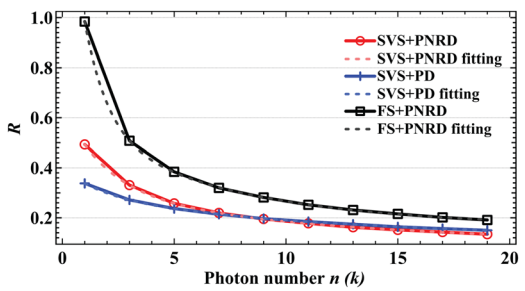

FIG. 5. The ratio R as the function of average photon number for various schemes. Here, we have chosen the detection photon number $k=n$. The red (circle) line denotes the "SVS + PNRD" and blues (cross) line and black (diamond) line the "SVS + PD" and "FS + PNRD," respectively. The dashed lines are fittings (see Ref. 26).

Now consider the minimum detected displacement, i.e., the sensitivity of the FPI. As is well known, classically, the precision in these experiments is limited by the limitation $1/N^{1/2}$ with N being the number of probes (photons and atoms) employed in the experiment. This limit is given by SQL. Quantum metrology provides the possibility of overcoming this limit when the entangled probes are used. There are many scenarios which can surpass the SQL and reach the HL given by $1/N$.[27–29] The sensitivity is also studied for FPI by SVS and non-Gaussian measurement.

For the FPI, the general uncertainty δL of a length measurement can be written as

$$\delta L = \frac{\Delta\hat{O}}{|\partial\langle\hat{O}\rangle/\partial L|}, \tag{7}$$

where $\langle\hat{O}\rangle$ is the mean value of the detection operator and $\Delta\hat{O}$ is the standard deviation of the observable $\hat{O}$. The operators of $\hat{a}^{+}\hat{a}$, $\hat{C}$, and $\hat{\Pi}$ for the detection of MID, PNRD, and PD, respectively, is defined as observable $\hat{O}$, which will be discussed below. For the SQL of FPI measured by MID, it is

$$\delta L_{\bar{n}}^{CS} = \frac{|t|}{\sqrt{\bar{n}}|\partial|t|^2/\partial L|}. \tag{8}$$

Using the definition of Eq. (7), the sensitivity for above-mentioned schemes of "SVS + PNRD" and "SVS + PD" becomes

$$\delta L_{PNRD}^{SVS} = \frac{\sqrt{P_k^{SVS}(1-P_k^{SVS})}}{\frac{1}{\cosh s}\sum_{j=0}^{\infty}\frac{[(2m)!]^2(\tanh s)^{2j}}{2^{2j}\cdot(j!)^2\cdot(2j-k)!\cdot k!}\partial\left(|t|^{2k}|r|^{2(2m-k)}\right)/\partial L}, \tag{9}$$

$$\delta L_{PD}^{SVS} = \frac{\sqrt{1-\left(P_{PD}^{SVS}\right)^2}}{\frac{1}{\cosh s}\sum_{m=0}^{\infty}\sum_{j=0}^{2m}\frac{[(2m)!]^2(\tanh s)^{2m}}{2^{2m}\cdot(m!)^2\cdot(2m-j)!\cdot j!}e^{i\pi j}\partial\left(|t|^{2k}|r|^{2(2m-k)}\right)/\partial L}. \tag{10}$$

The numerical results are illustrated in Fig. 6. For comparison, the corresponding sensitivity for "FS + PNRD" scheme was discussed in Ref. 16, and they demonstrated that such a scheme can improve upon SNL. The zoom in Fig. 6(b) tells a few strategies that can go beyond the shot noise limit (the dashed-dotted line), which include "SVS + PNRD" (red line), "SVS + PD" (black line), and "FS + PNRD" (blue line). However, the best performances are obtained by "SVS + PD" and "FS + PNRD," and these two schemes have the same sensitivities around the resonant point of FPI, while the former scheme "SVS + PD" has wider range of super sensitivity. On the whole, the use of both the quantum states and the quantum detection (here the non-Gaussian detection) show advantages and are superior to that of sole use of either quantum states or quantum detection. Nevertheless, there is still an exception. The "FS + PD" scheme can never exceed the SNL. That means that the eventual performance of quantum enhanced metrology, at least from the specific system that has been discussed here, is strongly dependent on the quantum resources, the detection strategies, and the specific design configurations. The general rules of quantum enhanced metrology for given quantum resources have yet to be established.

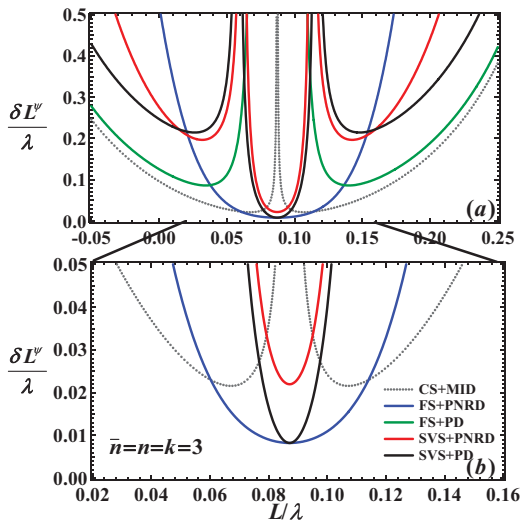

FIG. 6. The uncertainty $\delta L^{\psi}/\lambda$ as the function of L/λ with the detection photon number $k=n=3$ for different schemes. The black dotted line: CS + CD; the blue line: FS + PNRD; the green line: FS + PD; the red line: SVS + PNRD; the black line: SVS + PD. (b) The zoom of (a).

Thus, the non-classical source with appropriate detection methods can indeed realize the super sensitivity measurement. It proves again that quantum enhanced performance of FPI by using simultaneously the SVS input and non-Gaussian detection is feasible, and these schemes show great potential in the field of quantum enhanced metrology.

The paper has focused on the bandwidth of the transmission spectra and the sensitivity of a FPI by SVS injection based on the PNRD and PD. It shows that in any case the use

of SVS with two quantum detections, either "SVS + PNRD" or "SVS + PD," can improve the resolution of FPI and realize the super-resolution. Only the use of the SVS with classical detection, the CNB could not be improved any more. We also investigated quantitatively the bandwidth dependence on different photon detection and different average mean photon numbers, and the optimal performance that the scheme can reach has been discussed. If the PNRD technique alone is used, the appropriate photon number must be chosen to beat the CNB either injecting quantum light or classical light.

In addition, the uncertainty for length measurement of the FPI has been investigated. It indicates that the SVS with PD can realize the super sensitivity measurement. It is well known that quantum states can be used in quantum-enhanced measurement in some strategies, such as SVS, but if quantum detection is simultaneously used, such as the PNRD and PD of the non-Gaussian measurement, the measurement precision could be further improved. The joint use of various quantum light resources and the detection strategies could open up the way for quantum-enhanced measurement, which could be used for ultra-sensitive measurement, quantum imaging and quantum lithography.

This research work was supported by the National Natural Science Foundation of China (Grant Nos. 11125418, 91336107, 61275210, 61227902 and 61121064) and National Major Scientific Research Program of China (Grant No. 2012CB921601).

[1]P. M. Anisimov, G. M. Raterman, A. Chiruvelli, W. N. Plick, S. D. Huver, H. Lee, and J. P. Dowling, Phys. Rev. Lett. **104**, 103602 (2010).
[2]J. P. Dowling, Contemp. Phys. **49**, 125 (2008).
[3]M. Xiao, L. A. Wu, and H. J. Kimble, Phys. Rev. Lett. **59**, 278 (1987).
[4]K. Banaszek, R. D. Dobrzaski, and I. A. Walmsley, Nat. Photonics **3**, 673 (2009).
[5]V. Giovannetti, S. Lloyd, and L. Maccone, Nat. Photonics **5**, 222 (2011).
[6]V. Giovannetti, S. Lloyd, and L. Maccone, Science **306**, 1330 (2004).
[7]B. L. Higgins, D. W. Berry, S. D. Bartlett, H. M. Wiseman, and G. J. Pryde, Nature **450**, 393 (2007).
[8]M. Napolitano, M. Koschorreck, B. Dubost, N. Behbood, R. J. Sewell, and M. W. Mitchell, Nature **471**, 486 (2011).
[9]V. Giovannetti, S. Lloyd, and L. Maccone, Phys. Rev. Lett. **96**, 010401 (2006).
[10]C. M. Caves, Phys. Rev. Lett. **45**, 75 (1980).
[11]M. D. Lang and C. M. Caves, Phys. Rev. Lett. **111**, 173601 (2013).
[12]LIGO Scientific Collaboration, Nat. Phys. **7**, 962 (2011).
[13]J. Aasi, J. Abadie, B. P. Abbott *et al.*, Nat. Photonics **7**, 613 (2013).
[14]M. Mehmet, S. Ast, T. Eberle, S. Steinlechner, H. Vahlbruch, and R. Schnabe, Opt. Express **19**, 25763 (2011).
[15]R. H. Hadfield, Nat. Photonics **3**, 696 (2009).
[16]C. F. Wildfeuer, A. J. Pearlman, J. Chen, J. Y. Fan, A. Migdall, and J. P. Dowling, Phys. Rev. A **80**, 043822 (2009).
[17]A. J. Pearlman, A. Ling, E. A. Goldschmidt, C. F. Wildfeuer, J. Fan, and A. Migdall, Opt. Express **18**, 6033 (2010).
[18]T. C. Zhang, K. W. Goh, C.-W. Chou, P. Lodahl, and H. J. Kimble, Phys. Rev. A **67**, 033802 (2003).
[19]C. C. Gerry, A. Benmoussa, and R. A. Campos, Phys. Rev. A **72**, 053818 (2005).
[20]C. C. Gerry and J. Mimih, Contemp. Phys. **51**, 497 (2010).
[21]W. N. Plick, P. M. Anisimov, J. P. Dowling, H. Lee, and G. S. Agarwal, New J. Phys. **12**, 113025 (2010).
[22]J. Beyer and L. Ferrari, Supercond. Sci. Technol. **24**, 085004 (2011).
[23]Y. Li, G. Li, Y. C. Zhang, X. Y. Wang, J. Zhang, J. M. Wang, and T. C. Zhang, Phys. Rev. A **76**, 013829 (2007).
[24]Y. Q. Guo, R. C. Yang, G. Li, P. F. Zhang, Y. C. Zhang, J. M. Wang, and T. C. Zhang, J. Phys. B: At., Mol. Opt. Phys. **44**, 205502 (2011).
[25]The results fit very well with the empirical function of $f(k) = a + be^{-ck} + de^{-ek}$, which is shown as the dashed black curve in Fig. 4 with parameters: $a = 0.12$; $b = 0.76$; $c = 0.22$; $d = 12.03$; $e = 3.27$. It is expected that in the limit of $k \to \infty$, $R \to 0.12$.
[26]The results can be expected in the same way as the above discussion by the empirical formula (see Ref. 22). The expected values of $R = 0.17$ for "FS + PNRD", $R = 0.11$ for "SVS + PD," and $R = 0.094$ for "SVS + PD" are obtained when the photon number $n \to \infty$.
[27]J. Beltran and A. Luis, Phys. Rev. A **72**, 045801 (2005).
[28]S. Boixo, S. T. Flammia, C. M. Caves, and J. M. Geremia, Phys. Rev. Lett. **98**, 090401 (2007).
[29]J. P. Paz and A. J. Roncaglia, Phys. Rev. Lett. **100**, 220401 (2008).